Kernel-based Image Reconstruction from Radon data[1]

Stefano De Marchi

Department of Mathematics
University of Padova - Italy

December 7th, 2016

[1] *Work done in several years with various collaborators*

Main references

1. S. De Marchi, A. Iske and A. Sironi, *Kernel-based Image Reconstruction from Scattered Radon Data*, Dolomites Res. Notes on Approx. Vol 9, special issue for the workshop *Kernel-based methods and function approximation*, pp. 19–31.
2. T. G. Feeman, *The mathematics of medical imaging: a beginners guide* , Springer 2010.
3. Amos Sironi, *Medical image reconstruction using kernel-based methods*, Master's thesis, University of Padua, 2011, arXiv:1111.5844v1.
4. Davide Poggiali, *Reconstruction of medical images from Radon data in trasmission and emission tomography*, Master's thesis, University of Padua, 2012.
5. Maria Angela Narduzzo, *A kernel method for CT reconstruction: a fast implementation using circulant matrices*, Master's thesis, University of Padua, Dec. 2013.
6. Silvia Guglielmo, *Stable kernel based methods for medical image reconstruction*, Master's thesis, University of Padua, Dec. 2013.
7. Gabriele Santin,*Approximation in kernel-based spaces, optimal subspaces and approximation of eigenfunctions,* Padua Research ID: 9186, Ph.D. thesis (2016). Advisor: Stefano De Marchi.

Part I

The problem and the first approach

Work with A. Iske, A. Sironi

Outline

Description of CT
How does it work?

- Non-invasive medical procedure (X-ray equipment).
- X-ray beam is assumed to be:
  - monochromatic;
  - zero-wide;
  - not subject to diffraction or refraction.
- Produce cross-sectional images.
- Transmission tomography (emissive tomography, like PET and SPECT, are not considererd here)

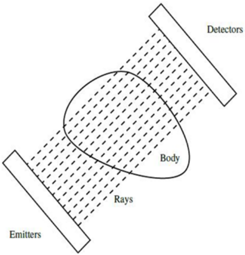

Description of CT
How does it work?

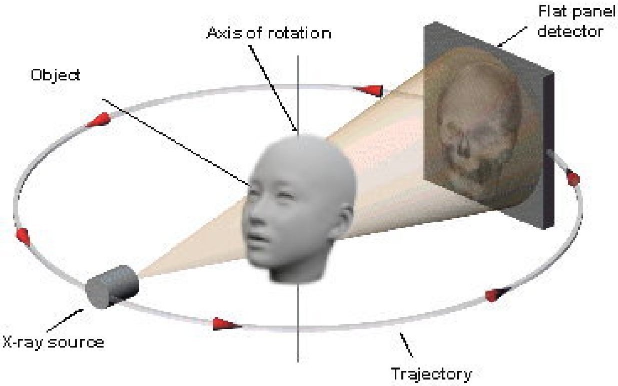

- $\ell_{(t,\theta)} \longrightarrow$ line along which the X-ray is moving;
- $(t,\theta) \in \mathbb{R} \times [0,\pi) \longrightarrow$ polar coordinates of line-points;
- $f \longrightarrow$ attenuation coefficient of the body;
- $I \longrightarrow$ intensity of the X-ray.

X-rays

- Discovered by Wihelm Conrad Röntgen in 1895
- Wavelength in the range $[0.01, 10] \times 10^{-9}$ m
- Attenuation coefficient:

$$
\begin{aligned}
A(x) &\approx \text{"}\#pho.s\ absorbed / 1\ mm\text{"} \\
A: &\quad \Omega \to [0, \infty)
\end{aligned}
$$

Figure : First X-ray image: Frau Röntgen left hand.

CT: people

Computerized Tomography (CT)

modern CT

Allan Mcleod Cormack

Godfrey Newbold Hounsfield

both got Nobel Price for Medicine and Physiology in 1979

Computerized Axial Tomography

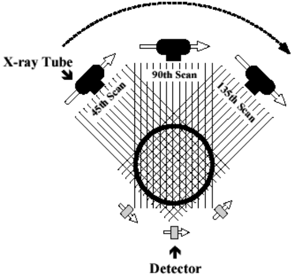

Figure : First generation of CT scanner design.

- A. Cormack and G. Hounsfield 1970
- Reconstruction from X-ray images taken from 160 or more beams at each of 180 directions
- Beer's law (loss of intensity):

$$\int_{x_0}^{x_1} A(x)\,dx = \underbrace{\ln\left(\frac{I_0}{I_1}\right)}_{\text{given by CT}}$$

Outline

Lines in the plane

A line l in the plane, perpendicular to the unit vector $\mathbf{n} = (\cos\theta, \sin\theta)$ and passing through $p = (t\cos\theta, t\sin\theta) = t\mathbf{n}$, can be characterized (by the polar coordinates $t \in \mathbb{R}$, $\theta \in [0, \pi)$), i.e. $l = l_{t,\theta}$

$$l_{t,\theta} = \{\mathbf{x} := (t\cos\theta - s\sin\theta, t\sin\theta + s\cos\theta) = (x_1(s), x_2(s)) \;\; s \in \mathbb{R}\}$$

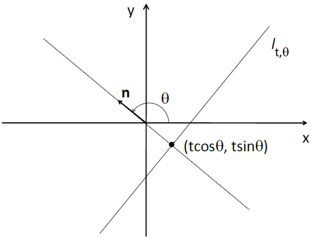

Figure : A line in the plane.

Radon transform
definition

The Radon transform of a given function $f : \Omega \subset \mathbb{R}^2 \to \mathbb{R}$ is defined for each pair of real number (t, θ), as line integral

$$Rf(t,\theta) = \int_{l_{t,\theta}} f(\mathbf{x}) d\mathbf{x} = \int_{\mathbb{R}} f(x_1(s), x_2(s))\, ds$$

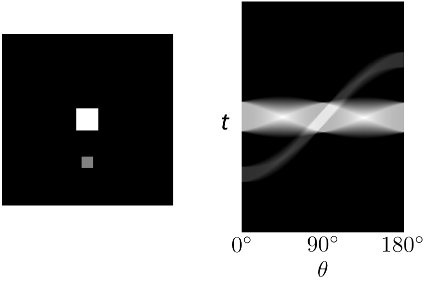

Figure : Left: image. Right: its Radon transform (*sinogram*)

Radon tranform
Image reconstruction

A CT scan measures the X-ray projections through the object, producing a sinogram, which is effectively the Radon transform of the attenuation coefficient function f in the (t, θ)-plane.

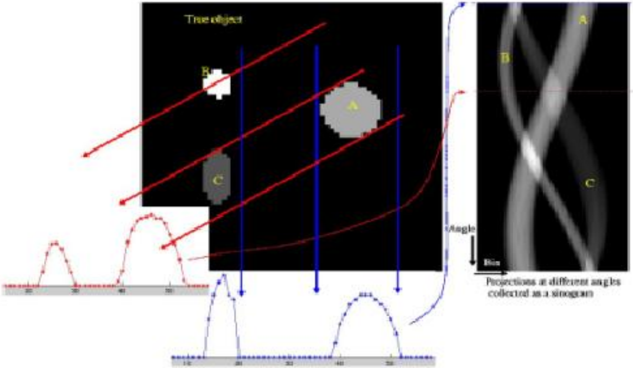

Radon transform: another example

Figure : Shepp-Logan phantom.

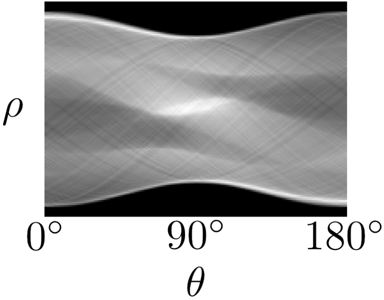

Figure : Radon transform (*sinogram*).

Back projection

- First attempt to recover f from Rf
- The back projection of the function $h \equiv h(t, \theta)$ is the transform

$$Bh(\mathbf{x}) = \frac{1}{\pi} \int_0^{\pi} h(x_1 \cos\theta + x_2 \sin\theta, \theta)\, d\theta$$

i.e. the average of h over the angular variable θ, where $t = x_1 \cos\theta + x_2 \sin\theta = \mathbf{x} \cdot \mathbf{n}$.

Figure : Back projection of the Radon transform.

Important theorems

Theorem (*Central Slice Theorem*)

For any suitable function f defined on the plane and all real numbers r, θ

$$F_2 f(r\cos\theta, r\sin\theta) = F(Rf)(r,\theta).$$

(F_2 and F are the 2-d and 1-d Fourier transforms, resp.).

Theorem (*The Filtered Back-Projection Formula*)

For a suitable function f defined in the plane

$$f(\mathbf{x}) = \frac{1}{2} B\{F^{-1}[|r| F(Rf)(r,\theta))]\}(\mathbf{x}), \quad \mathbf{x} \in \mathbb{R}^2.$$

Fundamental question

Fundamental question of image reconstruction.

Is it possible to reconstruct a function f starting from its Radon transform Rf? □

Answer (Radon 1917).

Yes, we can if we know the value of the Radon transform for all r, θ. □

Discrete problem

Ideal case

- $Rf(t,\theta)$ known for all t,θ
- Infinite precision
- No noise

Real case

- $Rf(t,\theta)$ known only on a finite set $\{(t_j,\theta_k)\}_{j,k}$
- Finite precision
- Noise in the data

Fourier-based approach

- Sampling: $Rf(t,\theta) \;\rightarrow\; R_D f(jd, k\pi/N)$
- Discrete transform: e.g.

$$B_D h(\mathbf{x}) = \frac{1}{N}\sum_{k=0}^{N-1} h(x\cos(k\pi/N) + y\sin(k\pi/N), k\pi/N)$$

- Filtering (low-pass): $|r| = F\phi(r)$, with ϕ band-limited function
- Interpolation: $\{f_k : \; k \in \mathbb{N}\} \;\rightarrow\; If(x), \; x \in \mathbb{R}$

Discrete problem

- Back-Projection Formula

$$f(\mathbf{x}) = \frac{1}{2} B\{F^{-1}[|r| \cdot F(Rf(r,\theta))]\}(\mathbf{x})$$

- Filtering

$$\begin{aligned} f(\mathbf{x}) &= \frac{1}{2} B\{F^{-1}[F(\phi(r)) \cdot F(Rf(r,\theta))]\}(\mathbf{x}) = \\ &= \frac{1}{2} B\{F^{-1}[F(\phi * Rf(r,\theta))]\}(\mathbf{x}) \\ &= \frac{1}{2} B[\phi * Rf(r,\theta)](\mathbf{x}) \end{aligned}$$

- Sampling and interpolation

$$f(x_1^m, x_2^n) = \frac{1}{2} B_D I[\phi * R_D f(r_j, \theta_k)](x_1^m, x_2^n)$$

Discrete problem: an example

Figure : Shepp-Logan phantom.

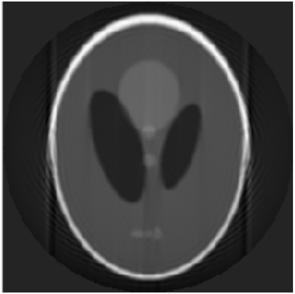

Figure : Reconstruction with linear interpolation and $180x101 = 18180$ samples.

Outline

Algebraic Reconstruction Techniques (ART)

Differently from Fourier-based reconstruction, we fix a set $\mathcal{B} = \{b_i\}_{j=1}^{n}$ of basis functions.

Example

A square image ($m = K^2$) can be expressed as

$$I(\mathbf{x}) = \sum_{i=1}^{m} a_i b_i(\mathbf{x}),$$

where

- a_i is the color of the i-th pixel,
- b_i the pixel basis, for $i = 1, \ldots, m$ given as

$$b_i(\mathbf{x}) = \begin{cases} 1 & \text{if } \mathbf{x} \text{ lies in pixel } i \\ 0 & \text{otherwise} \end{cases}$$

Linear system

- Asking

$$RI(t_j,\theta_j) = Rf(t_j,\theta_j), \quad j = 1,\ldots,n$$

we obtain the linear system

$$\sum_{i=1}^{m} a_i Rb_i(t_j,\theta_j) = Rf(t_j,\theta_j), \quad j = 1,\ldots,n$$

- Large but sparse linear system (usually rectangular)
- Solution by iterative methods (Kaczmarz, MLEM, OSEM, LSCG), or SIRT techniques (see also the Matlab package **AIRtools** by Hansen &Hansen 2012).

ART reconstruction: Example 1

Figure : Bull's eye phantom.

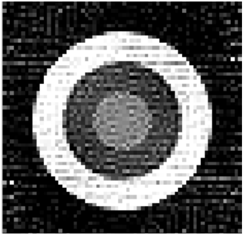

Figure : $64 \times 64 = 4096$ reconstructed image with 4050 samples by Kaczmarz.

ART reconstruction: Example 2

Figure : Shepp-Logan phantom.

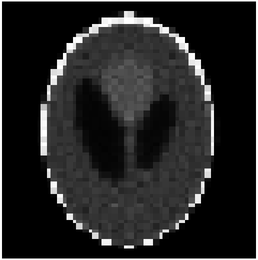

Figure : The phantom reconstructed by MLEM in 50 iterations.

Hermite-Birkhoff (H-B) (generalized) interpolation

Let $\Lambda = \{\lambda_1, \ldots, \lambda_n\}$ be a set of linearly independent linear functionals and $f_\Lambda = (\lambda_1(f), \ldots, \lambda_n(f))^T \in \mathbb{R}^n$.
The solution of a general H-B reconstruction problem:

H-B reconstruction problem

find $g = \sum_{j=1}^n c_j g_j$ such that $g_\Lambda = f_\Lambda$, that is

$$\lambda_k(g) = \lambda_k(f), \quad k = 1, \ldots, n\,. \tag{1}$$

Being $\lambda_k := R_k f = Rf(t_k, \theta_k), \quad k = 1, \ldots, n$ the conditions (1)

$$\sum_{j=1}^n c_j \lambda_k(g_j) = \lambda_k(f), \quad k = 1, \ldots, n \tag{2}$$

that corresponds to the linear system $A\mathbf{c} = \mathbf{b}$ as before.

H-B interpolation: basis functions

- Haar-Maierhuber-Curtis theorem (1904, 1956, 1959): In the multivariate setting, the well-posedness of the interpolation problem of scattered data is garanteed if we no longer fix in advance the set of basis functions.
- Thus, the basis g_j should depend on the data

$$g_j(\mathbf{x}) = \lambda_j^y(K(\mathbf{x},\mathbf{y}))\ \left[= R^{\mathbf{y}}[K(\mathbf{x},\mathbf{y})](t_k,\theta_k)\right], \quad j = 1,\ldots,n$$

chosing the kernel K such that the matrix

$$A = (\lambda_j^{\mathbf{x}}[\lambda_k^{\mathbf{y}}(K(\mathbf{x},\mathbf{y}))])_{j,k}$$

is not singular $\forall\ (t_k,\theta_k)$.

Positive definite radial kernels

We consider continuous kernels $K : \mathbb{R}^2 \times \mathbb{R}^2 \to \mathbb{R}$ s.t.

- Symmetric $K(\mathbf{x}, \mathbf{y}) = K(\mathbf{y}, \mathbf{x})$
- Radial $K(\mathbf{x}, \mathbf{y}) = \Phi_\epsilon(\|\mathbf{x} - \mathbf{y}\|_2), \ \epsilon > 0$
- Positive definite (PD)

$$\sum_{k,j=1}^{n} c_j c_k \lambda_j^{\mathbf{x}} \lambda_k^{\mathbf{y}} K(\mathbf{x}, \mathbf{y}) \geq 0$$

for all set of linear operators λ_j and for all $c \in \mathbb{R}^n \setminus \{0\}$

Kernel-based Image Reconstruction

Stefano De Marchi

Positive definite kernels: examples

- Gaussian

$$\Phi_\epsilon(\|\mathbf{x}\|) = e^{-(\epsilon\|\mathbf{x}\|)^2}, \quad PD \;\forall\, \mathbf{x} \in \mathbb{R}^2, \epsilon > 0$$

- Inverse multiquadrics

$$\Phi_\epsilon(\|\mathbf{x}\|) = \frac{1}{\sqrt{1 + (\epsilon\|\mathbf{x}\|)^2}}, \quad PD \;\forall\, \mathbf{x} \in \mathbb{R}^2,\; \epsilon > 0$$

- Askey's compactly supported (or radial characteristic function)

$$\Phi_\epsilon(\|\mathbf{x}\|) = (1 - \epsilon\|\mathbf{x}\|)_+^\beta = \begin{cases} (1 - \epsilon\|\mathbf{x}\|)^\beta & \|\mathbf{x}\| < 1/\epsilon \\ 0 & \|\mathbf{x}\| \geq 1/\epsilon \end{cases}$$

which are PD for any $\beta > 3/2$.

A useful Lemma

Lemma

Let $K(\mathbf{x},\mathbf{y}) = \Phi(\|\mathbf{x}-\mathbf{y}\|_2)$ *with* $\Phi \in L^1(\mathbb{R})$*. Then for any* $\mathbf{x} \in \mathbb{R}^2$ *the Radon transform* $R^{\mathbf{y}}K(\mathbf{x},\mathbf{y})$ *at* $(t,\theta) \in \mathbb{R} \times [0,\pi)$ *can be expressed*

$$(R^{\mathbf{y}}K(\mathbf{x},\mathbf{y}))(t,\theta) = (R^{\mathbf{y}}K(\mathbf{0},\mathbf{y}))(t-\mathbf{x}\cdot\mathbf{n},\theta)\,.$$

$\longrightarrow$ shift invariant property of the Radon transform.

Problem

- Inverse multiquadric kernel

$$K(\mathbf{x}, \mathbf{y}) = \frac{1}{\sqrt{1 + \|\mathbf{x} - \mathbf{y}\|_2^2}}.$$

Applying the previous Lemma we have

$$R^{\mathbf{y}}[K(\mathbf{0}, \mathbf{y})](t, \theta) = \int_{\mathbb{R}} \frac{1}{\sqrt{1 + t^2 + s^2}} \, ds = +\infty$$

Hence, the basis g_k and the matrix A are not well defined!

Regularization

Window function

- Multiplying the kernel K by a window function w such that

$$R[K(\mathbf{x},\mathbf{y})w](t,\theta) < \infty \; \forall \; (x,y),(t,\theta).$$

- This corresponds to use the linear operator R_w in place of R

$$R_w[f](t,\theta) = R[fw](t,\theta).$$

- We consider w radial, $w = w(\|\cdot\|_2)$

Example of window functions

- Characteristic function

$$w(\mathbf{x}) = \chi_{[-L,L]}(\|\mathbf{x}\|_2),\ L > 0$$

- Gaussian

$$w(\mathbf{x}) = e^{-\nu^2\|\mathbf{x}\|_2^2},\ \nu > 0$$

- Compactly supported (Askey's family)

$$w(\mathbf{x}) = (1 - \nu^2\|\mathbf{x}\|_2^2)_+,\ \nu > 0$$

Example: Gaussian kernel

- Gaussian kernel, shape parameter ε

$$K(\mathbf{x},\mathbf{y}) = e^{-\varepsilon^2 \|\mathbf{x}-\mathbf{y}\|_2^2}, \ \varepsilon > 0$$

- Basis function

$$g_j(\mathbf{x}) = R^{\mathbf{y}}[K(\mathbf{x},\mathbf{y})](t_j,\theta_j) = \frac{\sqrt{\pi}}{\varepsilon} e^{-\varepsilon^2 (t_j - x\cdot v_j)^2}$$

with $v_j = (\cos\theta_j, \sin\theta_j)$

- Matrix $A = (a_{k,j})$

$$a_{k,j} = R[g_j](t_k,\theta_k) = +\infty, \quad \text{if } \theta_j = \theta_k$$

Example: Gaussian kernel (cont')

- Considering the Gaussian window function

$$w(\mathbf{x}) = e^{-\nu^2 \|\mathbf{x}\|_2^2}, \ \nu > 0$$

- The matrix A becomes

$$a_{k,j} = R[g_j w](t_k, \theta_k) = \frac{\pi \exp\left[-\nu^2 \left(t_k^2 + \frac{\varepsilon^2 \beta^2}{\varepsilon^2 \alpha^2 + \nu^2}\right)\right]}{\varepsilon \sqrt{\varepsilon^2 \alpha^2 + \nu^2}}$$

where $\alpha = \sin(\theta_k - \theta_j)$ and $\beta = t_j - t_k \cos(\theta_k - \theta_j)$

Example: Gaussian kernel (cont')

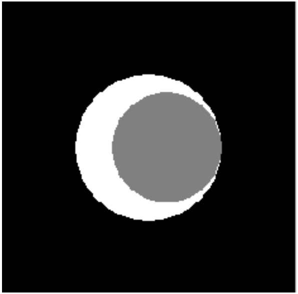

Figure : Crescent-shaped phantom.

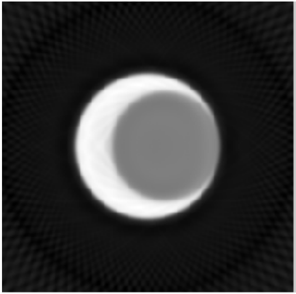

Figure : $256 \times 256 = 65536$ reconstructed image with $n = 4050$ samples.

A numerical experiment

- Gaussian kernel Φ_ϵ and gaussian weight w_ν
- Comparison with the Fourier-based reconstruction (relying on the FBP)
- Reconstructions from scattered Radon data and noisy Radon data
- Root Mean Square Error

$$RMSE = \frac{1}{J}\sqrt{\sum_{i=1}^{J}(f_i - g_i)^2}$$

J is the dimension of the image, $\{f_i\}, \{g_i\}$ the greyscale values at the pixels of the original and the reconstructed image.

Kernel-based vs Fourier based: I

◇ Test phantoms

Figure : crescent shape

Figure : bull's eye

Figure : Shepp-Logan

Geometries

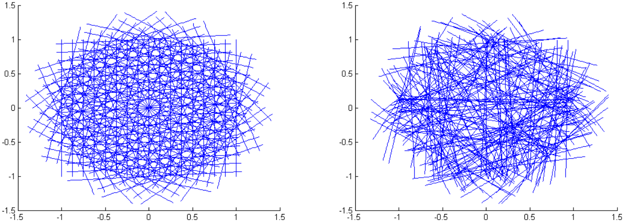

Figure : Left: parallel beam geometry, 170 lines (10 angles and 17 Radon lines per angle). Right: scattered Radon lines, 170 lines.

Kernel-based vs Fourier based: II

- Using parallel beam geometry, i.e.
  $\theta_k = k\pi/N,\ k = 0,\dots,N-1$ and $t_j = jd,\ j = -M,\dots,M,$
  with sampling spacing $d > 0 \longrightarrow (2M+1)\times N$ regular grid of Radon lines. No noise on the data.
- With $N = 45,\ M = 40,\ \epsilon = 60$ we got

Phantom	optimal ν	kernel-based	Fourier-based
crescent	0.5	0.102	0.120
bull's eye	0.4	0.142	0.134
Shepp-Logan	1.1	0.159	0.177

Table : RMSE of kernel-based vs Fourier-based method

Kernel-based vs Fourier based: III

- Using scattered Radon data, with increasing randomly chosen Radon lines $n = 2000, 5000, 10000, 20000$. No noise on the data.
- With $\epsilon = 50$ and $\nu = 0.7$ we got

Phantom	2000	5000	10000	20000
crescent	0.1516	0.1405	0.1431	0.1174
bull's eye	0.1876	0.1721	0.2102	0.1893

Table : RMSE of kernel-based vs different number n of Radon lines

Kernel-based vs Fourier based: IV

- These experiments are with noisy Radon data, i.e. we add a gaussian noise of zero mean and variance $\sigma = 1.e-3$ to each of the three phantoms.
- With same parallel beam geometry and same ϵ and ν

Phantom	kernel-based	Fourier-based
crescent	0.1502	0.1933
bull's eye	0.1796	0.2322
Shepp-Logan	0.1716	0.2041

Table : RMSE of kernel-based vs Fourier-based with noisy data

- With scattered Radon data and same ϵ and ν

Phantom	noisy	noisy-free
crescent	0.2876	0.1820
bull's eye	0.3140	0.2453

Table : RMSE with noisy and noisy-free data

Window function parameter

- Gaussian kernel; Gaussian window function

$$K(\mathbf{x},\mathbf{y}) = e^{-\varepsilon^2\|\mathbf{x}-\mathbf{y}\|_2^2} \qquad w(\mathbf{x}) = e^{-\nu^2\|\mathbf{x}\|_2^2}$$

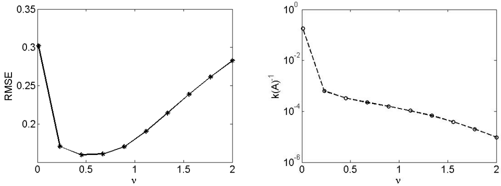

(a) *RMSE* (b) $k^{-1}(A)$

Figure : Bull's eye phantom, $\varepsilon = 30$.

- Trade-off principle (Schaback 1995)

Kernel shape parameter

- Multiquadric kernel, Gaussian window

$$K(\mathbf{x},\mathbf{y}) = \sqrt{1+\rho^2\|\mathbf{x}-\mathbf{y}\|_2^2}\, e^{-\varepsilon^2\|\mathbf{x}-\mathbf{y}\|_2^2}$$

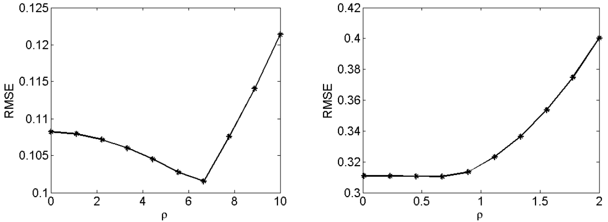

(a) Crescent-shaped phantom (b) Shepp-Logan phantom

Figure : Optimal values depend on the data.

Comparison with FBP Formula

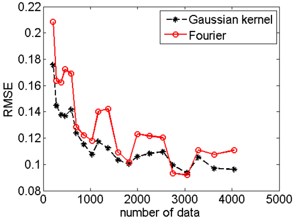

Figure : FBP and Gaussian kernel reconstruction (with optimal parameters ε^*, ν^*).

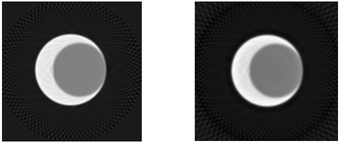

(a) (b)

Figure : Crescent-shaped: (a) FBP; (b) Gaussian kernel.

Comparison with FBP Formula

* *RMSE* of the same order (ok!)
* More computational time and memory usage (not so well!)

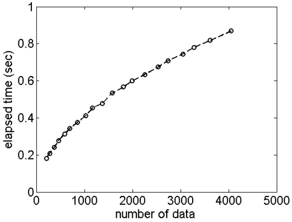

(a) FBP

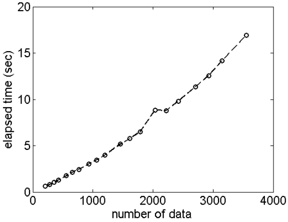

(b) Multiquadric kernel

Figure : Computational time.

Part II

Fast implementation of ART

Work with F. Filbir, J. Frikel and M. Narduzzo

Algebraic Reconstruction Technique (ART): generality

- ART determines a solution in the recovery subspace

$$\boxed{S_\Upsilon := \mathrm{span}\,\{\Phi_\epsilon(\cdot - y_j) : 1 \le j \le J\} \subseteq N_\Phi(\Omega)},$$

  where $\Upsilon := \{y_1, \ldots, y_J\} \subseteq \Omega$ arbitrary, but fixed, set of reconstruction points and $\{\Phi_\epsilon(\cdot - y_j)\}_{j=1}^J$ translates of the basis function Φ (RBFs).

- Search solution for $R\,f = \bar{g}$ of the form

$$\boxed{\tilde{f}_\Upsilon = \sum_{j=1}^J \alpha_j \Phi_\epsilon(\cdot - y_j) \in S_\Upsilon},$$

  with $\alpha = (\alpha_1, \ldots, \alpha_J)^T \in \mathbb{R}^J$ to be determined.

Thanks to the linearity of the Radon transform ...

ART-problem

Search a solution $\tilde{\alpha} \in \mathbb{R}^J$ for the linear system

$$\boxed{A\alpha = \bar{g}},$$

where $A \in \mathbb{R}^{KL \times J}$ is the collocation matrix defined as

$$A_{i(k,l),j} := R\left(\Phi(\cdot - y_j)\right)(t_k, \theta_l)$$

for $1 \leq i(k,l) \leq KL$ and $1 \leq j \leq J$.

Theorem

Let $A \in \mathbb{R}^{KL \times J}$ and $\bar{g} \in \mathbb{R}^{KL}$. Then,

1. *There is* at least *one solution of the minimization problem*

$$\boxed{\min_{\alpha \in \mathbb{R}^J} |A\alpha - \bar{g}|}.$$

   There exists exactly *one solution with minimal Euclidean norm (Moore-Penrose solution α^+).*

2. *The solution comes from the system of normal equations*

$$\boxed{A^T A\alpha = A^T \bar{g}}.$$

$M := A^T A$ $\underline{\text{symmetric}}$ and $\underline{\text{positive definite}}$

M $\underline{\text{non-singular}}$

$\exists!$ solution for $M\alpha = \widetilde{g}$
with $\widetilde{g} := A^T \bar{g}$

$M\alpha = \widetilde{g}$ solve with e.g. CGM

Theorem

Let $M \in \mathbb{R}^{J\times J}$ be a positive definite matrix. For any $\alpha^{(0)} \in \mathbb{R}^J$, the sequence $\left\{\alpha^{(k)}\right\}_{k\in\mathbb{N}}$, generated by the CGM, converges to the minimal norm solution α^+ in at most J steps.

The matrix-vector product performed in $O(J \cdot KL)$ floating-points operations.

Fast implementation

Choose a polar reconstruction grid

$$\boxed{\Upsilon_{D_N,\Theta} := \left\{ y_{j(n,\tilde{l})} = r_n(\cos(\theta_{\tilde{l}}), \sin(\theta_{\tilde{l}}))^T : 1 \leq j(n,\tilde{l}) \leq NL \right\}},$$

with

$$D_N := \{r_n \in [-r, r] : \Delta r > 0 \ \text{ for } 1 \leq n \leq N\}$$

and

$$\Theta := \left\{ \theta_{\tilde{l}} \in [0, \pi) : \Delta\theta > 0 \ \text{ for } 1 \leq \tilde{l} \leq L \right\}$$

s.t. Θ is the set of angular coordinates of the line-points.

Fast implementation of ART

Efficient choice of reconstruction points

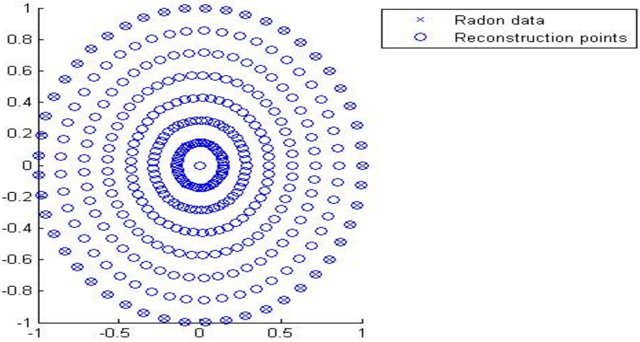

Line-points with radius 1 (asterisks). Polar reconstruction grid in $B_1(0) \subseteq \mathbb{R}^2$ (small circles).

BLOCK CIRCULANT STRUCTURE for A

$$A = \begin{bmatrix} A_{11} & \dots & A_{1N} \\ \vdots & \ddots & \vdots \\ \vdots & \ddots & \vdots \\ A_{K1} & \dots & A_{KN} \end{bmatrix} \in \mathbb{R}^{KL \times NL}$$

where every block-matrix $A_{kn} \in \mathbb{R}^{L \times L}$ takes the form

$$A_{kn} = \begin{bmatrix} a_1 & a_2 & \dots & \dots & a_{L-1} & a_L \\ a_L & a_1 & a_2 & \dots & \dots & a_{L-1} \\ \vdots & a_L & a_1 & \dots & \dots & \vdots \\ a_3 & \ddots & \ddots & \ddots & \ddots & a_2 \\ a_2 & a_3 & \dots & \dots & a_L & a_1 \end{bmatrix} \in \mathbb{R}^{L \times L}$$

Fast implementation of ART

Fast matrix-vector product using a circulant matrix

Theorem (Main theorem, Narduzzo master's thesis)

Let $C \in \mathbb{R}^{L\times L}$ be a circulant matrix with first column $c \in \mathbb{R}^L$. Further, let $F_L \in \mathbb{C}^{L\times L}$ be the rescaled Fourier matrix ($F_{i,j} = \frac{1}{\sqrt{L}}\mu_L^{(i-1)(j-1)}$ with $\mu_L := e^{-\frac{2\pi i}{L}}$). Let F_L^* be its conjugate transpose. Then, it holds

$$\boxed{C\,v = F_L^*[(F_L\,c)\odot(F_L\,v)] \quad \forall v \in \mathbb{R}^L}. \tag{3}$$

Here $\odot$ is the component-wise multiplication operator: $x \odot y = (x_1y_1, \dots, x_Ly_L), \quad x, y \in \mathbb{R}^L$.

Matrix-vector product now performed in

$$\boxed{O(NKL\lg(L)) \text{ floating-points operations}}$$

through the use of **FFT** and **IFFT**.

Choice of the RBF

RBF: Gaussian with shape parameter $\epsilon > 0$

$$\Phi_\epsilon(x-y) := e^{-\epsilon^2\|x-y\|^2} \; \forall x, y \in \mathbb{R}^2.$$

Entries of the collocation matrix:

$$\begin{aligned} A_{i(k,l),j(n,\tilde{l})} &= R\Phi_\epsilon(\cdot - y_{j(n,\tilde{l})})(t_k, \theta_l) \\ &= \frac{\sqrt{\pi}}{\epsilon} e^{-\epsilon^2(t_k - r_n\cos(\theta_l - \theta_{\tilde{l}}))^2} \end{aligned}$$

for $1 \le i(k,l) \le KL$ and $1 \le j(n,\tilde{l}) \le NL$.

Experiment 1

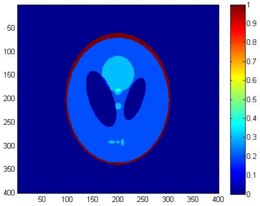

Shepp-Logan phantom.

$L \times K = 360 \times 569$ (angular $\times$ radial)
$N = 150$ (Δr $cost$);
$\epsilon = 150$;
$iter = 30$;
$R = 400$ (resolution).

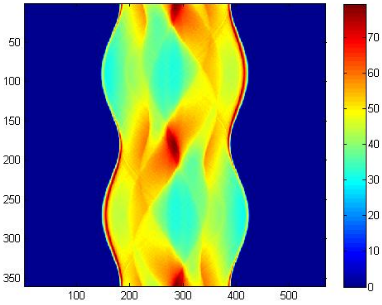

Computational efficiency...

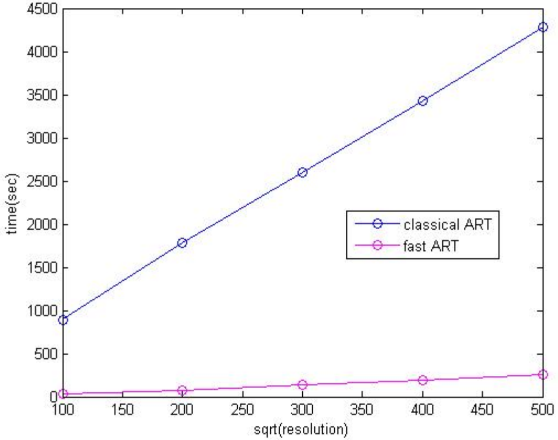

CPU time plot (in sec) as a function of the available Radon data, $\widetilde{R}$

Numerical results

Experiment 1: Computational efficiency and accuracy of FCGM

$R = 400$; $L \times K = 360 \times 569$.

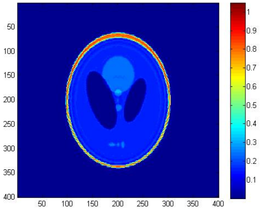

Reconstructed phantom

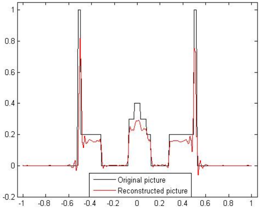

Cross-section (line 180)

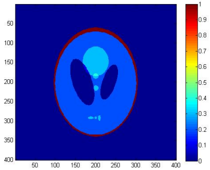

Original phantom

Numerical results
Experiment 1-Equispaced vs fast Leja radii

$$RMSE = 0.076764$$
$$max\text{-}err = 1.045491$$
$$CPU\ \ time = 274.5\ sec$$

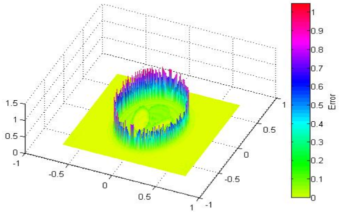

Error plot (equispaced radii)

$$RMSE = 0.080900$$
$$max\text{-}err = 1.086950$$
$$CPU\ \ time = 284.9\ sec$$

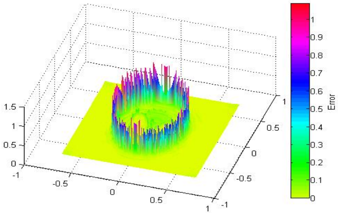

Error plot (fast Leja radii)

Experiment 2

$\kappa(B) :=$ ℓ^2-*condition number*;

$q_\Upsilon :=$ *separation distance* between reconstruction points;

$h_{\mathfrak{X},\Delta} :=$ *fill-distance* line-points $\mathfrak{X}$;

$q_{\mathfrak{X},\Upsilon} :=$ *separation distance* between line-points and reconstruction points.

* From several experiments we obtained ($C > 0, \tau > \frac{d}{2}$)

$$\boxed{\|\widetilde{f}_\Upsilon - f\|_2 \leq C \left(h_{\mathfrak{X},\Delta} \cdot q_{\mathfrak{X},\Upsilon}\right)^\tau \left(1 + \sqrt{\kappa(B)}\right) \|f\|_{N_{\Phi_\epsilon(\Omega)}}},$$

* From theoretical results on RBF we know ($C_d > 0$) [(cf. Fasshauer's book)]

$$\boxed{\kappa(B) = \lambda_{\max}/\lambda_{\min}},$$

$$\boxed{\lambda_{\max} \leq (NL) \cdot \Phi_\epsilon(0)}, (\textit{Gerschgorin's theorem})$$

$$\boxed{\lambda_{\min} \geq C_d \left(\sqrt{2}\epsilon\right)^{-d} e^{-40.71 d^2/(q_\Upsilon \epsilon)^2} q_\Upsilon^{-d}}.$$

Smiley phantom;
$L \times K = 144 \times 171$.

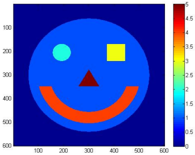

$iter = 30$;
$R = 100$.

$\boxed{N \text{ variable } (\Delta r \ cost); \qquad \bar{\epsilon} = 60}$

N *n.rec.circles*	L^2 *error*	λ_{min} *min.eigenvalue*	$\kappa(B)$ *cond.number*
40	41.081787	$1.081460 \cdot 10^{-19}$	$5.032868 \cdot 10^{20}$
50	35.247683	$3.592425 \cdot 10^{-30}$	$1.948570 \cdot 10^{31}$
55	36.214269	$1.998062 \cdot 10^{-30}$	$7.207981 \cdot 10^{31}$
60	33.359540	$1.292076 \cdot 10^{-31}$	$6.739194 \cdot 10^{32}$
65	33.087770	$4.161096 \cdot 10^{-32}$	$3.469419 \cdot 10^{33}$
80	33.476398	$9.725620 \cdot 10^{-33}$	$1.276718 \cdot 10^{34}$

Numerical results

Experiment 2: Trade-off numerical stability vs accuracy (stationary case)

Smiley phantom;
$L \times K = 144 \times 171$.

$iter = 30$;
$R = 100$.

$\boxed{\epsilon > 0 \text{ variable}; \quad \bar{N} = 30 \ (\Delta r \ cost)}$

ϵ shape par.	L^2 error	λ_{min} min.eigenvalue	$\kappa(B)$ cond.number
30	43.746117	$2.792255 \cdot 10^{-31}$	$3.054914 \cdot 10^{32}$
35	44.580586	$4.402922 \cdot 10^{-31}$	$1.616392 \cdot 10^{32}$
40	45.708660	$9.237581 \cdot 10^{-28}$	$6.632798 \cdot 10^{28}$
45	47.903512	$2.764322 \cdot 10^{-25}$	$1.950951 \cdot 10^{26}$
50	52.583766	$2.059636 \cdot 10^{-24}$	$2.341632 \cdot 10^{25}$

Numerical results

Experiment 3: Choice of reconstruction parameters

Experiment 3

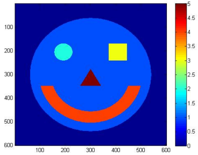

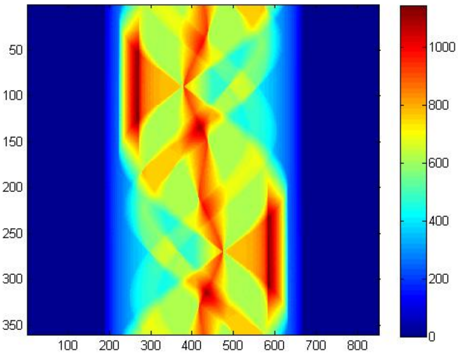

Smiley phantom;

$L \times K = 360 \times 811$.

$R = 600$;
$\epsilon = ?$;
$N = ?$;
$iter = ?$.

1) Best shape parameter... $iter = 30$

$N = 75$ (Δr $cost$) $N = 150$ (Δr $cost$)

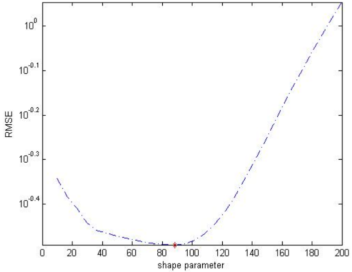

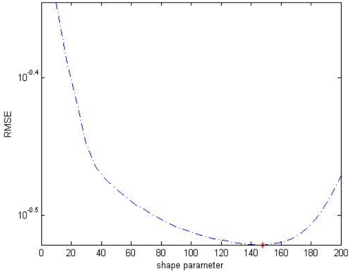

RMSE as a function of ϵ for equispaced reconstruction radii $N = 75$ (left) and $N = 150$ (right).

...Heuristic rule.. $\left(\Delta r := \frac{1}{N}\right)$

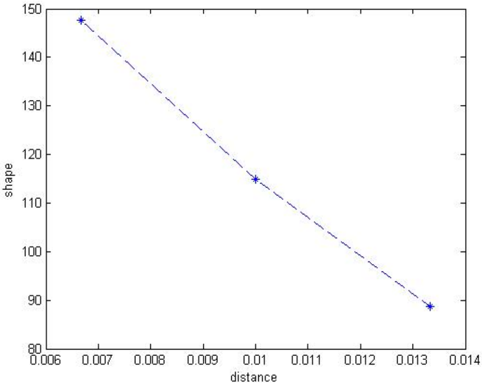

$$\boxed{\epsilon \approx -9\,828 \cdot \Delta r + 216}$$

2) Best number of reconstruction circles...

$$iter = 20; \; \Delta r \; cost$$

N *n. rec.circles*	*N·L* *n. rec.points*	ϵ *shape param.*	*RMSE*	*maximal error*	*CPU time (seconds)*
50	18 000	19.440	0.408572	4.053001	101.7
75	27 000	84.960	0.317973	4.409125	134.0
100	36 000	117.720	0.300916	4.237258	181.8
125	45 000	137.376	0.295240	3.958031	237.7
150	**54 000**	**150.480**	**0.297035**	**4.309017**	**309.1**
175	**63 000**	**159.840**	**0.296148**	**3.543423**	**384.0**
200	**72 000**	**166.860**	**0.295511**	**3.624649**	**486.0**
225	81 000	172.320	0.295141	3.512590	594.3
250	90 000	176.688	0.296305	3.638046	668.8

RMSE and CPU time for increasing larger sets of reconstruction points.

$$\boxed{\text{for } R = 600, \text{ from } N = 150 \text{ to } N = 200}$$

3) Different iteration steps...

$$N = 200\ (\Delta r\ cost); \quad \epsilon = 160$$

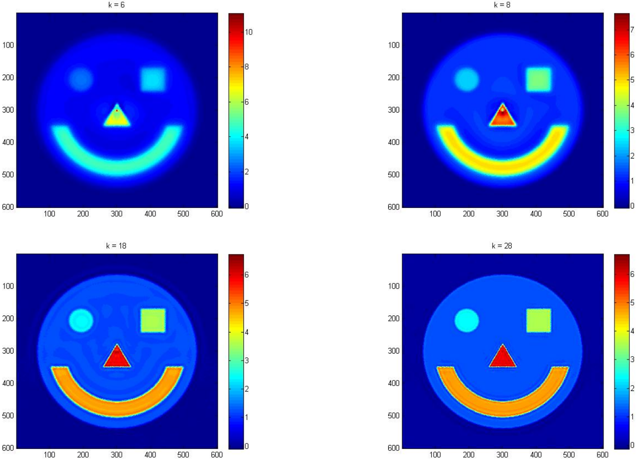

Numerical results

Experiment 3: Choice of number of iterations

$$RMSE = 0.291745 \qquad max\text{-}err = 3.614396$$
$$CPU\ \ time = 527.8\,\text{sec}$$

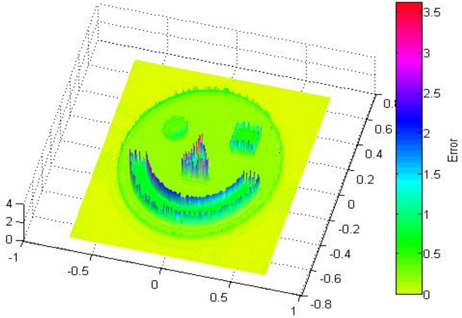

Error plot for $iter = 28$.

...Stopping condition...

$N = 200$ (Δr *cost*); $\epsilon = 160$

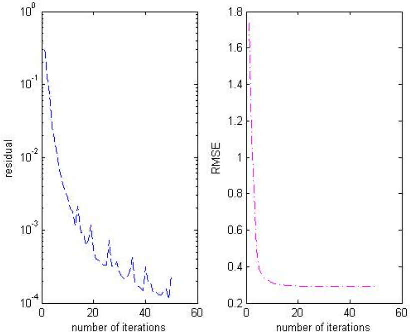

Convergence history of residual and RMSE respect to the number of iterations.

$\boxed{tol = 10^{-3} \text{ for the residual decrease}}$

Experiment 4

10% white Gaussian noise

Shepp-Logan phantom;

$L \times K = 360 \times 711$.

$N = 150$ (Δr *cost*);
$\epsilon = 150.48$;
$iter = 25$;

$R = 500$.

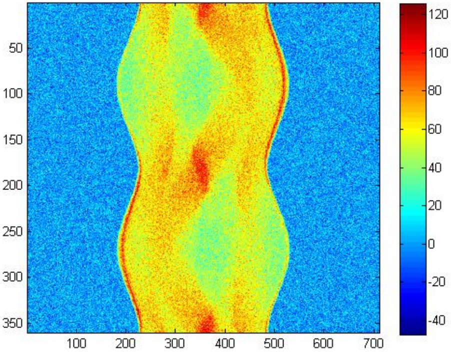

Numerical results

Experiment 4: Noisy data

$$RMSE = 0.101538 \qquad max\text{-}err = 1.310516$$

$$residual\text{-}decrease = 10^{-2} \qquad CPU\ \ time = 298.3\,\text{sec}$$

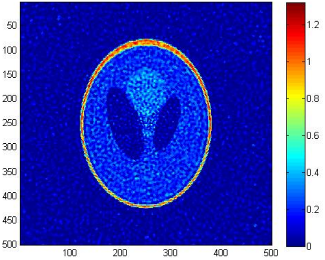

Reconstructed phantom

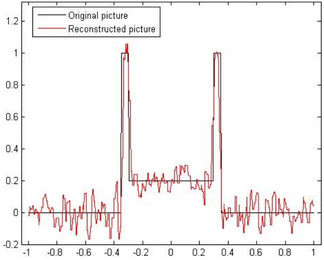

Cross-section (line 120)

Experiment 5

human pelvis;

$L \times K = 2\,304 \times 736$.

$N = 200$ (Δr *cost*);
$\epsilon = 166.86$;
$tol = 10^{-3}$;
$R = 520$.

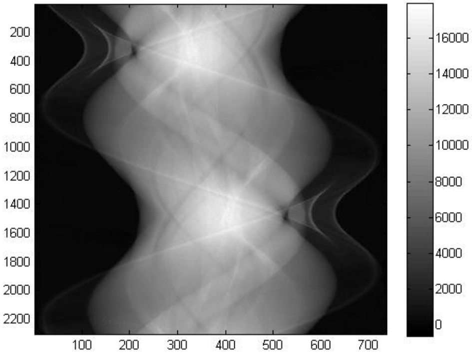

Data provided by Department of Diagnostic and Interventional Radiology at TUM

Numerical results

Experiment 5: Real experimental data

$NRMSE(A\alpha^{(k)}, \bar{g}) = 0.034964$ $\quad$ $residual\text{-}decrease = 10^{-3}$

$iter = 22$ $\quad$ $CPU\ \ time = 14\,027.2\,\text{sec}$

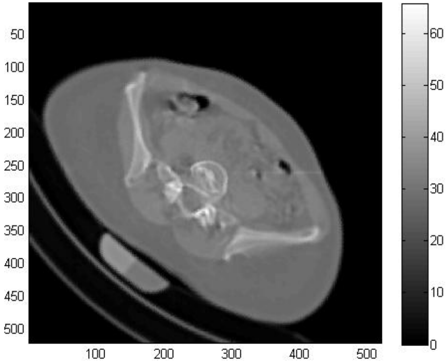

Reconstructed image

Conclusions

Conclusions...

BLOCK CIRCULANT STRUCTURE

⬇

FAST MATRIX-VECTOR PRODUCT

⬇

FAST CGM

⬇

FAST ART

⬇

MORE COMPUTATIONAL EFFICIENCY!
SAME IMAGE RECONSTRUCTION CAPABILITY!

Thank you for your attention!